ACS APPLIED MATERIALS & INTERFACES

www.acsami.org

Research Article

Predictions of Chemical Shifts for Reactive Intermediates in CO_2 Reduction under *Operando* Conditions

Hao Yang,[▽] Fabio Ribeiro Negreiros,[▽] Qintao Sun, Miao Xie, Luca Sementa, Mauro Stener, Yifan Ye, Alessandro Fortunelli,* William A. Goddard, III,* and Tao Cheng*

Cite This: *ACS Appl. Mater. Interfaces* 2021, 13, 31554–31560

Read Online

ACCESS | Metrics & More | Article Recommendations | Supporting Information

ABSTRACT: The electroreduction of CO_2 into value-added products is a significant step toward closing the global carbon loop, but its performance remains far from meeting the requirement of any practical application. The insufficient understanding of the reaction mechanism is one of the major causes that impede future development. Although several possible reaction pathways have been proposed, significant debates exist due to the lack of experimental support. In this work, we provide opportunities for experiments to validate the reaction mechanism by providing predictions of the core-level shifts (CLS) of reactive intermediates, which can be verified by the X-ray photoelectron spectroscopy (XPS) data in the experiment. We first validated our methods from benchmark calculations of cases with reliable experiments, from which we reach consistent predictions with experimental results. Then, we conduct theoretical calculations under conditions close to the *operando* experimental ones and predict the C 1s CLS of 20 reactive intermediates in the CO_2 reduction reaction (CO_2RR) to CH_4 and C_2H_4 on a Cu(100) catalyst by carefully including solvation effects and applied voltage (U). The results presented in this work should be guidelines for future experiments to verify and interpret the reaction mechanism of CO_2RR.

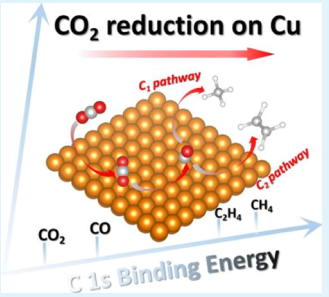

KEYWORDS: *carbon loop, CO_2 reduction reaction, chemical shifts, reactive intermediates*

1. INTRODUCTION

As a typical greenhouse gas, the rapid growth of CO_2 emission, associated with the evolution of developed economies and the consequent rapid growth of energy resources and the chemical industry, has been demonstrated to play an important role in inducing drastic climate change.[1] Substantial progress in decarbonization methods is strongly needed at present in order to close the carbon cycle, that is, to reduce net CO_2 emissions rapidly.[2] Among them, the electrochemical reduction of CO_2 to useful organics (such as formate, methane, ethylene, ethanol, *etc.*) is of considerable importance to nature and motivates research interests in areas such as energy, chemistry, and materials science.[3,4] In particular, a significant amount of research focusing on copper (Cu) materials has been conducted because Cu, among many transition metals, is unique in reducing CO_2 to hydrocarbons in a sizable amount.[5−7] Electrocatalysis is a powerful way to successfully conduct CO_2 reduction reaction (CO_2RR), but the lack of molecular-based understanding of the reactive intermediate and reaction pathways at the electrode−electrolyte interface (EEI) is a significant impediment to future development. Several well-established experimental techniques, such as surface-enhanced Raman scattering spectroscopy (SERS),[8,9] ambient-pressure X-ray photoelectron spectroscopy (APXPS),[10−12] and so on, have been used to investigate the process of CO_2 reduction reactions, but it is difficult to clarify the mechanism of variable deep-reduction products, particularly when separating short-term reaction intermediates due to the limitation of experimental resolution. In short, the understanding of the electrochemical CO_2RR mechanism is still far from satisfactory, which hinders progress in the field.

Various reaction mechanisms of CO_2RR on Cu have been proposed based on experimental observations and theoretical models.[13−15] In general, it is likely that the step for adsorption and activation of CO_2 (*i.e.*, $*CO_2$) is the starting point for CO_2RR, but there is still some uncertainty on which is the first intermediate in the next step, namely, whether the intermediate binds the proton (hydrogenation) through the carbon atom or oxygen atom (*COOH *vs* *OCHO intermediates), leading to the CO and formate pathways, respectively.[16,17] For deep products (such as C_2H_4), the reaction mechanism is even more ambiguous. Until now, it is generally agreed that CO is the primary intermediate in the formation of C_1 and C_{2+} compounds, but all the reaction mechanisms after CO formation are still unclear.[14] Usually, the major selectivity between the C_1 and C_{2+} pathways is the competition between the hydrogenation mechanism and the dimerization process, based on the pH as

Received: February 11, 2021
Accepted: June 15, 2021
Published: June 29, 2021

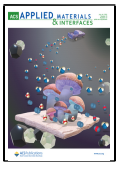

https://doi.org/10.1021/acsami.1c02909
ACS Appl. Mater. Interfaces 2021, 13, 31554−31560

found in the experiment.[18] In previous work, we have theoretically suggested[19] complete reaction pathways of CO, CH_4, and C_2H_4 formation, but these predictions need to be validated by experimental results thus far not available.

In order to facilitate development and provide guidance on the design of catalysts with enhanced performance, our strategy is to provide a full atomistic understanding of how CO_2 interacts with and transforms on the electrode surfaces. More importantly, we plan to correlate these predictions directly with the experimental *operando* characterization of the established reaction intermediates using a variety of spectroscopic techniques, such as IR, Raman, and X-ray photoelectron spectroscopy (XPS). We have thus carried out full explicit solvent QM-based MD to characterize more than 20 reactive intermediates involved in carbon dioxide reduction and subsequent carbon monoxide reduction reactions on the Cu(100) surface (CO_2RR and CORR, respectively). Since these QM-MD characterizations were carried out at 298 K with explicit consideration of the solvent and applied voltage,[19] the simulation results can be compared directly with *operando* experiments, providing a systematic, straightforward interpretation of the experimental data.[20] Many QM calculations have been reported with the atomistic insight of the reaction mechanism of CO_2RR. However, previous studies were deficient in not fully including solvent effects. For example, early calculations ignored the solvent in the simulation,[21,22] while later studies[15] used a variety of implicit solvation models that do not include the role of hydrogen bonding by the solvent. In contrast, our simulations use five layers of explicit water to ensure that they can be compared to *operando* experiments and to ensure that the reactions at the catalyst−solvent interface are properly treated. Previously, we have predicted vibrational signatures of CO_2RR on Cu(100),[20] but to achieve a complete picture with full validation and understanding and to resolve interpretation, including cases with vibrational signatures definitively overlapping, rigorous information on XPS data is mandatory.

To provide a basis for comparing with *operando* atmospheric pressure XPS experiments, we predict here the C 1s XPS binding energy based on QM-MD at 298 K in explicit solution to characterize all plausible species generated during the reduction process. We do provide a complete picture of spectroscopic signatures of CO_2RR at the Cu(100) surface to trigger experimental efforts in this field. We expect that this will help us to guide experimental studies of reaction pathways and dramatically accelerate the development and design of new electrocatalysts.

2. COMPUTATIONAL DETAILS

2.1. VASP AIMD Simulations. Here, we simulate the water/Cu(100) interface using 48 explicit water molecules (five layers, 1.21 nm-thick) on a 4 × 4 Cu(100) surface slab (three layers) with an area of 1.02 nm^2. To equilibrate the waters interacting with the interface, we carried out 2 ns reactive molecular dynamics (R.M.D.) simulations using the reactive force field (ReaxFF) with parameters for Cu and H_2O.[23] Starting from this well-equilibrated interface, we carried out 10 ps *ab initio* molecular dynamics (AIMD) simulation at 298 K. We find that including one extra Na solvated in the solution leads to a work function of 3.40 (±0.25) eV, which corresponds to −0.59 V (R.H.E.) (3.40 − 4.40 + 0.0592 × 7 = −0.59 V), close to the potential [−0.60 V (R.H.E.)] with maximum C_2H_4 production at pH 7.[24] The simulation box is 40 Å along the *z*-axis with a vacuum of 24 Å. The lateral dimensions of the slab were fixed using a lattice parameter of 3.61 Å. Two CO molecules and one H atom were placed on the 4 × 4 unit cell (on the top site), corresponding to a surface coverage of 1/8 ML and 1/16 ML, respectively. A snapshot of the simulation box is shown in the Supporting Information (Figure S1). We consider that this model of QM with an explicit treatment of the water dynamics at *operando* condition temperature provides a representative description of the reaction kinetics.

Electronic structure calculations were performed within the framework of density functional theory (DFT), as implemented in the Vienna *ab initio* simulation program (VASP) of version 5.4.4.[25−28] The exchange and correlation energies were calculated using the Perdew, Burke, and Ernzerhof (PBE) functionals within the generalized gradient approximation (GGA).[29,30] Projector augmented wave potentials represented core electrons. Spin polarization did not have an appreciable effect on the overall energies. For example, the total energies are different by less than 0.01 eV for adsorbed hydrogen (*H) on the Cu(100) surface. The calculations were therefore carried out without spin polarization to reduce computational demands.

We used a plane-wave cutoff energy of 400 eV and the first-order Methfessel−Paxton scheme with a smearing width of 0.2 eV. Dipole corrections were applied along the *z*-axis. The PBE-D3 method was employed to correct van der Waals interactions of water−water and water−Cu.[31] The energy minimization criterion was that all forces on free atoms were <0.02 eV/Å.

We used a 1.2 fs time step in the molecular dynamics (MD) simulations with the hydrogen mass set to 2 atomic mass units. These MD simulations used only the gamma point of the Brillouin zone without consideration of symmetry. The velocities were rescaled every 20 MD steps to readjust the target temperature to equilibrium. We employed a Nose−Hoover thermostat for the free energy calculations with a temperature damping parameter of 100 fs.

2.2. Prediction of the Core-Level Shift. The XPS simulations were conducted to predict the core-level energies of carbon atoms in equilibrated frames from the ab initio MD trajectory implemented in VASP at the PBE-D3 level. In VASP, there are two approaches for the calculation of the core-level shift (CLS)—the initial- and final-state approximation. The initial-state approximation is based on the Kohn−Sham (K.S.) eigenvalues of the core states after a self-consistent calculation of the valence charge density, while the final-state approximation requires removing the electron from the core and placing it into the valence.[32] We selected the initial-state method to predict the *relative* CLS because previous studies have shown that such an approach is reliable in reproducing the relative binding energy change as measured experimentally.[11,33] The work function's effect was not considered during the calculations (see Table S1 for more details). The s^2p2 electronic state of C was used for the CLS calculations. For directly comparing with the experimental observation, all the calculated CLSs were transformed to absolute values.

3. RESULTS AND DISCUSSION

In this work, we focus on Cu(100), which has been shown to be a stable surface under CO_2RR *operando* conditions, and it is known to be more active and selective toward C_2H_4, which is the most desirable among the CO_2RR products.[34] In our previous work,[19] we have predicted the reaction pathway of C_2H_4 formation as follows

https://doi.org/10.1021/acsami.1c02909
ACS Appl. Mater. Interfaces 2021, 13, 31554−31560

$$l\text{-}CO_2 \rightarrow b\text{-}CO_2 \rightarrow *COOH \rightarrow *CO \quad (1)$$

After *CO formation, the formation of C_2H_4 is as follows

$$*CO + *CO \rightarrow *OC{-}CO \rightarrow *OC{-}COH \rightarrow *HOC{-}COH \rightarrow *C{-}COH \rightarrow *CH{-}COH \rightarrow *C{-}CH \rightarrow *C{-}CH_2 \rightarrow *CH{-}CH_2 \rightarrow C_2H_4 \quad (2)$$

In this reaction pathway, two reactive intermediates are important: one is *CO that is the only confirmed reactive intermediate during CO_2RR and the other is *CO−CO, which facilitates the formation of the C_{2+} product by CO coupling.[14]

We are also interested in the formation of CH_4, which is another major hydrocarbon product. While Cu(111) is selective for the formation of CH_4,[18] CH_4 is also important on Cu(100). In our previous work,[19] we predict the reaction pathway of CH_4 formation as follows

$$*CO \rightarrow *CHO \rightarrow *CHOH \rightarrow *CH. \rightarrow *CH_2 \rightarrow *CH_3 \rightarrow *CH_4 \quad (3)$$

Note that CH_4 formation is also from CO. In this reaction pathway, *CHO is the important reactive intermediate that determines both the thermodynamics and kinetics. All the optimized structures for reactive intermediates and the applied potential (U) for each species are shown in Figure 1 and Table S2.

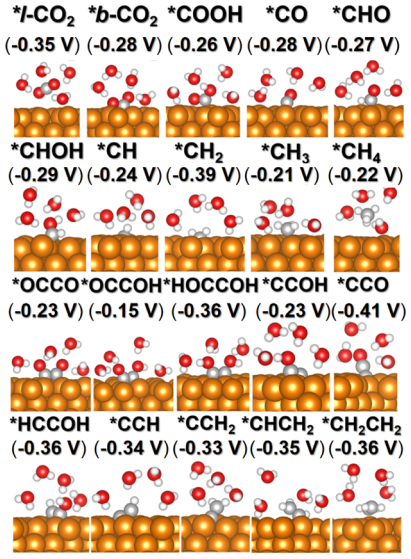

Figure 1. Optimized atomic structures of reactive intermediates in CO_2RR/CORR from AIMD simulations with five layers of explicit solvation. Colors are used as follows: Cu in orange, C in gray, O in red, and H in white. Only the water molecules in close contact are shown, while the other water molecules are removed for viewing convenience. The applied potentials for each species are shown in black brackets.

In order to benchmark the accuracy of the PBE functional in predicting the CLS, we compared multiple cases with available experimental data. The predictions and comparisons are shown in Table 1. To compare with the relative CLS, the gas-phase CO_2 is taken as a reference according to the experimental results. As shown in Figure 2, PBE with initial-state (PBE-I) approximation systematically underestimates the CLS when compared with experimental results. These underestimations come in part from the initial-state approximation and in part from the PBE functional. Since we must use a plane-wave, non-hybrid, non-charged approach to make AIMD on large periodic systems computationally practical, to account for the difference between a working and fully predictive DFT/CLS approach, we propose a local fragment similarity (LFS) procedure. Thus, we first investigate a prototypical set of gas-phase species using a final-state CLS approach, the B3LYP xc-functional,[35,36] and the ADF code,[37] employing a large basis set of Slater orbitals on PBE/D3-optimized geometries. The corresponding results reported in Table 1 and Figure 2 demonstrate that we can get fully predictive results *via* such final-state DFT/hybrid CLS simulations, with an accuracy of 0.1−0.2 eV in CLS predictions. We then employ a LFS procedure consisting of the following steps:

(1) For each chemically different adsorbate species, we select a representative geometry of that species on the surface of the catalyst.
(2) On the selected geometry, we freeze the coordinates of atoms of the adsorbate and remove all other atoms.
(3) We predict DFT/CLS values *via* both VASP/PW/PBE/initial-state and ADF/Slater/B3LYP/final-state approaches and derive the difference between these two values for each given adsorbate species, as reported in Table 2.
(4) We take the differences in CLS values in point (3) as best estimates of corrections due to intrinsic limitations of our working DFT/CLS method, and we use them to derive our best predictions of CLS values under *operando* conditions in Table 4 and Figure 3.

The advantage of PBE-I is its high efficiency, which provides a practical solution for a periodic system with hundreds of atoms. Such predictions can be systematically improved when a hybrid function calculation with final-state approximation (HFF) is ready for calculations with hundreds of atoms in a periodic box. Before that, we propose that a PEB-I calculation with a postage correction by referencing to HFF is the most efficient and accurate way to predict the CLS of electrochemical reactions.

The experimental measurement of XPS under *operando* conditions is very challenging for the experiment, but it is possible using our simulation approach. Thus, we report the CLS of all the reactive intermediates in the reaction pathway of CH_4 and C_2H_4 formation in advance of and to guide future experiments. The reactants, reactive intermediates, and products considered in this manuscript include *l-CO_2, *b-CO_2, *COOH, *CO, *CHO, *CHOH, *CH, *CH_2, *CH_3, *CH_4, *OCCO, *OCCOH, *HOCCOH, *CCOH, *CCO, *HCCOH, *CCH, *CCH_2, *$CHCH_2$, and *CH_2CH_2. In our previous work, we investigated energetics and kinetics carefully. At −0.6 V, we take 0.1 eV as a criterion because it roughly leads to a ratio between the reactant and product of 50:1. Otherwise, the product is too small to be significant. We thus predict that possible experimentally detectable species include *l-CO_2, *b-CO_2, *CO, and *CCO. The C 1s CLS of these species is predicted as 278.50, 277.27, 276.99, and 274.18 and 276.12, respectively, and is reported in Table 3. Qualitatively, as expected, the CLS values continuously decrease along the whole reduction process. Although the lifetimes of the other species are low on Cu(100), they may survive in specified sites on advanced catalysts, such as oxygen-derived Cu nanoparticles. We, therefore, provide all the predictions for future experimental validations.

All the predictions are collected in Figure 3 and Table 4. The reported CLS prediction is the average of 20 samples from a 10

https://doi.org/10.1021/acsami.1c02909
ACS Appl. Mater. Interfaces 2021, 13, 31554−31560

Table 1. Calculated and Experimental Binding Energy of C 1s Relative to $CO_{2(g)}$ [*i.e.*, R_{CLS} = (CLS-CO_2−CLS-Molecule)] for Selected Molecules as Benchmarks of Relevance for CO_2RR[a]

molecules	C	calculated (PBE-level)/eV[b]	calculated (B3LYP-level)/eV[c]	experimental/eV[38,39]
$CO_{2(g)}$		0[d]	0[d]	0[d]
CO		1.62	1.32	1.48
CH_4		5.38	6.97	6.80
CH_3OH		3.79	5.40	5.31
HCOOH		1.12	2.05	1.91
$C_2H_2(sp)$		4.65	6.57	6.50
$C_2H_4(sp^2)$		4.89	7.12	7.00
$C_2H_6(sp^3)$		5.30	7.22	6.90
CH_3COOH	$C_{(CH_3)}$	4.58	5.99	6.11
	$C_{(COOH)}$	1.34	2.54	2.33

[a]Simulated data are reported in the gas phases discussed in the text. [b]We put all these molecules into a large box (10 × 10 × 10 Å) and then calculated the core-level energy using the initial-state approach in VASP. [c]We calculated all these gas-phase molecules with the hybrid B3LYP method in ADF. [d]The binding energy for gas-phase CO_2 was set to 0 to get a relative value for the CLS.

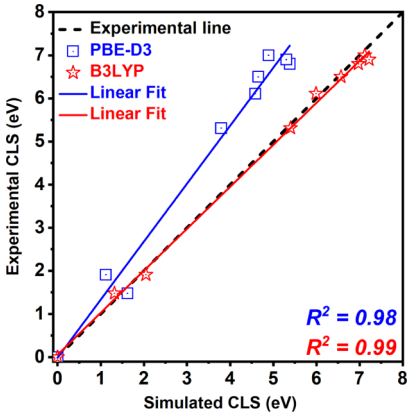

Figure 2. Relative energy differences of the C 1s CLS of eight molecules regarding gas-phase CO_2 (*i.e.*, set CLS_{CO_2} = 0) at the PBE (red) and B3LYP (blue) level compared to experimental values (solid black line at 0 eV).

ps NVT simulation with 500-step intervals. These XPS predictions can provide critical information to identify reactive intermediates.

- As a first striking outcome of our simulations, we find a 3.80 eV difference between CO_2(g) and *l*-CO_2. This is the result of the overall effect of solvation, adsorption, and applied voltage, with explicit solvation playing here the most important role, as proved by the fact that we find a similar shift also in the absence of the Cu(100) surface (as shown in Figure S2). This is a major prediction that awaits experimental validation.
- The 1.51 eV difference between *l*-CO_2 and *CO is a second major prediction that could also be validated by experiments in a relatively easy procedure since *CO is one of the stable intermediates, and both CO_2 and *CO can be produced experimentally by working at a bias just below the electrochemically active one.
- Third, since both *b*-CO_2 and *COOH have been proposed as possible intermediates in the path from CO_2 to CO and their CLS is 277.27 and 277.10 eV, respectively, signals in between *l*-CO_2 and *CO, if they are observed experimentally, can prove the existence of these reaction intermediates from CO_2 to CO and potentially even monitor their inter-conversion if sufficient experimental resolution is achieved.

Table 2. Binding Energy Differences of CO_2 and Subsequent CO_2RR Reductive Fragments Calculated by PBE and B3LYP, Respectively

fragments[a]	C 1s binding energy (PBE-level) (eV)		C 1s binding energy (B3LYP-level) (eV)		Exp. (eV)	unpaired electrons
l-CO2	0[b]		0[c]		0[d]	0
b-CO2	0.82		0.24			0
COOH	0.41		1.72			1
CO	1.27		1.06		1.48	0
CHO	1.31		2.62			1
CHOH	2.64		4.93			2
CH	2.05		4.94			3
CH_2	3.92		5.82			2
CH_3	4.69		5.61			1
CH_4	5.32		7.04		6.80	0
OC−CO	0.42		3.05			2
OC*x*−C*y*OH	C_x: 2.13	C_y: 1.23	3.05	C_y: 3.87		3
HOC−COH	2.87		5.85			2
C*x*=C*y*=O	C_x: 2.56	C_y: 0.98	C_x: 4.69	C_y: 2.78		2
C*x*−C*y*OH	C_x: 3.34	C_y: 2.22	C_x: 5.68	C_y: 4.44		1
C*x*H−C*y*OH	C_x: 3.81	C_y: 1.98	C_x: 6.78	C_y: 4.89		2
C*x*−C*y*H	C_x: 2.76	C_y: 3.12	C_x: 4.80	C_y: 5.17		1
C*x*−C*y*H2	C_x: 2.50	C_y: 4.17	C_x: 4.15	C_y: 6.22		0
C*x*H−C*y*H2	C_x: 3.96	C_y: 4.62	C_x: 6.42	C_y: 6.77		1
C_2H_4	4.71		7.04		7.00	0

[a]The geometries or 20 reactive fragments were taken from the surface species without all the Cu atoms and other solvent molecules. [b]Reference to CO_2 at PBE. [c]Reference to CO_2 at B3LYP. [d]Reference to CO_2 in the experiment.

- The most reactive intermediate in the CH_4 formation is *CHO, and its CLS is 276.63 eV, close to that of *CO, while the other intermediates (such as *CHOH, *CH, *etc.*) exhibit a CLS more significantly different from that of CO. These differences will be of help to distinguish *CHO from the other species and to determine the relative energy of CH_4.

https://doi.org/10.1021/acsami.1c02909
ACS Appl. Mater. Interfaces 2021, 13, 31554−31560

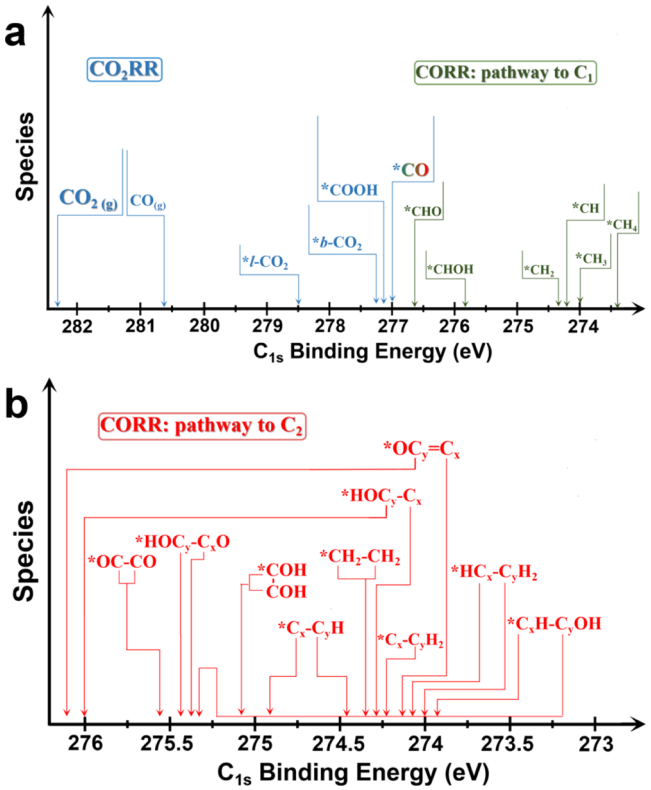

Figure 3. Calculated C 1s binding energy for 20 reactive intermediates in CO_2RR and CORR processes, (a) CO_2 reduction to C_1 pathway, and (b) CO reduction to C_2 pathway.

Table 3. Comparison of the Calculated C 1s Binding Energy for Important Reactive Intermediates in CO_2RR

species	C 1s binding energy (eV)	relative difference (eV)
CO_2(g)	282.30	0
*l-CO_2	278.50	3.80
*b-CO_2	277.27	5.03
*CO	276.99	5.31
*CHO	276.63	5.67
*OC−CO	275.51	6.79
*CCO	274.18, 276.12	8.12, 6.18

- The difference of CLSs between *CO and C_2H_4 is 2.63 eV. Interestingly, at variance with the pathway to CH_4, some of the intermediates (such as *C=C=O, *$CHCH_2$, *etc.*) in the C_2H_4 formation pathway exhibit larger chemical shifts than C_2H_4. In particular, *OC−CO has been predicted as one of the most important reaction intermediates.[19] The CLS of *OC−CO is 275.51 eV, which is well separated from that of either *CO or C_2H_4. Thus, XPS measurements should be able to distinguish *OC−CO from other intermediates univocally.

Overall, these XPS predictions set the stage for assigning the CLSs to important intermediate species and will be especially useful when resolution *via* experimental data alone is difficult.

We have reported the detailed relative free energies in our previous work.[17,19] Based on these free energy data, CO_2, CO, and products such as CH_4 are expected to be stable, while the other reactive intermediates are short-lived. Nevertheless, specified conditions, such as applied voltage, undercoordinated sites, and so on, are of help to stabilize specified intermediates and extend their lifetime, which provides opportunities for

Table 4. Calculated Binding Energy of CO_2 and Subsequent CO_2RR Reduction Intermediates on the Cu(100) Surface[a]

species	C 1s binding energy[b] (eV)	species	C 1s binding energy[b] (eV)	
*l-CO2	278.50	*OC−CO	275.51	
*b-CO2	277.27	*OCx−CyOH	C_x: 275.37	C_y: 275.43
*COOH	277.10	*HOC−COH	275.14	
*CO	276.99	*Cx=Cy=O	C_x: 274.18	C_y: 276.12
*CHO	276.63	*Cx−CyOH	C_x: 274.28	C_y: 276.00
*CHOH	275.81	*CxH−CyOH	C_x: 273.85	C_y: 275.36
*CH	274.19	*Cx−CyH	C_x: 274.88	C_y: 274.48
*CH_2	274.32	*Cx−CyH2	C_x: 274.55	C_y: 274.24
*CH_3	273.99	*C_xH−C$y$$H_2$	C_x: 274.10	C_y: 274.00
*CH_4	273.41	*C_2H_4	274.36	

[a]Where relevant, C_x and C_y distinguish two carbon atoms in different chemical environments in the same molecular species. [b]The C 1s binding energies for 20 reaction species on Cu(100) are obtained from the average value of core-level energy of 20 snapshots randomly taken from the QM-MD trajectory.

experimental characterization. In our previous work,[17] we predicted that at PZC (−0.38 V), l-CO_2 is 0.32 eV more stable than b-CO_2. Assuming that the electron transfer from l-CO_2 to b-CO_2 is 0.5 e^-, it is not changing significantly with U. Then, b-CO_2 becomes more stable when U is more negative than −1.02 V.

Noting that the solvent configurations in EDL are very sensitive to the distance to the interface, it is possible that the CLS of physisorbed species, such as CO_2, is also sensitive to the distance to the interface. Indeed, in our results, the comparison between gas-phase and operando predictions, for example, for CO_2, demonstrates that solvation plays an important role in stabilizing the excited species. Our current initial-state approximation does capture this, while future final-state simulations may provide better insights.

4. CONCLUSIONS

In summary, we carried out first-principles AIMD simulations to investigate the reactive intermediates in CO_2 reduction under *operando* conditions with explicit consideration of solvation and applied voltage effects. We propose a local fragment similarity (LFS) procedure in which the initial-state CLS approximation is improved with a postage correction by referencing to hybrid xc-functional DFT calculations with final-state effects (HFF) as an efficient and accurate way to predict the CLS of electrochemical reactions. The CLS of C 1s in 20 reaction intermediates was predicted at the DFT-PBE-D3 level. The analysis of the predicted XPS results showed a crucial effect of solvation on the CLS, with a downward shift of nearly 4 eV. It is also shown that it is possible to distinguish important reactive intermediates, such as *b-CO_2, *CHO, and *OC-CO, by taking l-CO_2, CO, C_2H_4, and CH_4 as references. Our predictions have a twofold goal: (i) to provide valuable information for the experiment to resolve and interpret the data from XPS measurements and (ii) to build up a reaction mechanism at the atomistic level that can be validated using several *independent and mutually complementing* characterization techniques, so as to solve the mechanistic

https://doi.org/10.1021/acsami.1c02909
ACS Appl. Mater. Interfaces 2021, 13, 31554−31560

questions still debated. The understanding of the reaction mechanism will pave the way to the rational design of advanced CO_2RR catalysts.

■ ASSOCIATED CONTENT

Supporting Information

The Supporting Information is available free of charge at https://pubs.acs.org/doi/10.1021/acsami.1c02909.

Atomic structure of the water/Cu(100) electrode, optimized structures of CO_2 and CO_2 + nH_2O, comparison of the calculated binding energy of the C 1s reference to vacuum, and coordinates for all predicted intermediates (PDF)

■ AUTHOR INFORMATION

Corresponding Authors

Alessandro Fortunelli − *CNR-ICCOM & IPCF, Consiglio Nazionale delle Ricerche, Pisa 56124, Italy; Materials and Process Simulation Center, California Institute of Technology, Pasadena, California 91125, United States;* orcid.org/0000-0001-5337-4450; Email: alessandro.fortunelli@cnr.it

William A. Goddard, III − *Materials and Process Simulation Center, California Institute of Technology, Pasadena, California 91125, United States;* orcid.org/0000-0003-0097-5716; Email: wag@caltech.edu

Tao Cheng − *Institute of Functional Nano & Soft Materials (FUNSOM), Jiangsu Key Laboratory for Carbon-Based Functional Materials & Devices, Joint International Research Laboratory of Carbon-Based Functional Materials and Devices, Soochow University, Suzhou 215123, Jiangsu, PR China;* orcid.org/0000-0003-4830-177X; Email: tcheng@suda.edu.cn

Authors

Hao Yang − *Institute of Functional Nano & Soft Materials (FUNSOM), Jiangsu Key Laboratory for Carbon-Based Functional Materials & Devices, Joint International Research Laboratory of Carbon-Based Functional Materials and Devices, Soochow University, Suzhou 215123, Jiangsu, PR China;* orcid.org/0000-0002-8241-6231

Fabio Ribeiro Negreiros − *CNR-ICCOM & IPCF, Consiglio Nazionale delle Ricerche, Pisa 56124, Italy; INFIQC, CONICET, Universidad Nacional de Córdoba, Córdoba 5000, Argentina*

Qintao Sun − *Institute of Functional Nano & Soft Materials (FUNSOM), Jiangsu Key Laboratory for Carbon-Based Functional Materials & Devices, Joint International Research Laboratory of Carbon-Based Functional Materials and Devices, Soochow University, Suzhou 215123, Jiangsu, PR China*

Miao Xie − *Institute of Functional Nano & Soft Materials (FUNSOM), Jiangsu Key Laboratory for Carbon-Based Functional Materials & Devices, Joint International Research Laboratory of Carbon-Based Functional Materials and Devices, Soochow University, Suzhou 215123, Jiangsu, PR China;* orcid.org/0000-0002-9797-1449

Luca Sementa − *CNR-ICCOM & IPCF, Consiglio Nazionale delle Ricerche, Pisa 56124, Italy*

Mauro Stener − *Dipartimento di Scienze Chimiche e Farmaceutiche, Università di Trieste, Trieste 34127, Italy;* orcid.org/0000-0003-3700-7903

Yifan Ye − *National Synchrotron Radiation Laboratory, University of Science and Technology of China, Hefei 230029, China*

Complete contact information is available at: https://pubs.acs.org/10.1021/acsami.1c02909

Author Contributions

$^{\nabla}$H.Y. and F.R.N. contributed equally to this work.

Notes

The authors declare no competing financial interest.

■ ACKNOWLEDGMENTS

TC was supported by the National Natural Science Foundation of China (grant no. 21903058), the Natural Science Foundation of Jiangsu Province (Grant go. BK20190810), Jiangsu Province High-Level Talents (JNHB-106), and China Postdoctoral Science Foundation (no. 2019M660128). This work was partly supported by the Collaborative Innovation Center of Suzhou Nano Science and Technology, the Priority Academic Program Development of Jiangsu Higher Education Institutions (PAPD), and the 111 Project. WAG was supported by the Liquid Sunlight Alliance, which is supported by the U.S. Department of Energy, Office of Science, Office of Basic Energy Sciences, Fuels from Sunlight Hub under Award Number DE-SC0021266. Computational support from CINECA Supercomputing Centre within the ISCRA program is gratefully acknowledged. AF and WAG received support from NSF (CBET-1805022).

■ REFERENCES

(1) Intergovernmental Panel on Climate Change. *Climate Change 2014: Synthesis Report*, 2014.

(2) Obama, B. The Irreversible Momentum of Clean Energy. *Science* **2017**, *355*, 126−129.

(3) Bagger, A.; Ju, W.; Varela, A. S.; Strasser, P.; Rossmeisl, J. Electrochemical CO2 Reduction: A Classification Problem. *ChemPhysChem* **2017**, *18*, 3266−3273.

(4) Liu, Y.; Qiao, J.; Zhang, J. *Electrochemical Reduction of Carbon Dioxide: Fundamentals and Technologies*, 1st ed.; C.R.C. Press, 2016.

(5) Nitopi, S.; Bertheussen, E.; Scott, S. B.; Liu, X.; Engstfeld, A. K.; Horch, S.; Seger, B.; Stephens, I. E. L.; Chan, K.; Hahn, C.; Nørskov, J. K.; Jaramillo, T. F.; Chorkendorff, I. Progress and Perspectives of Electrochemical CO_2 Reduction on Copper in Aqueous Electrolyte. *Chem. Rev.* **2019**, *119*, 7610−7672.

(6) Kuhl, K. P.; Cave, E. R.; Abram, D. N.; Jaramillo, T. F. New Insights into the Electrochemical Reduction of Carbon Dioxide on Metallic Copper Surfaces. *Energy Environ. Sci.* **2012**, *5*, 7050−7059.

(7) Hori, Y.; Kikuchi, K.; Suzuki, S. Production of CO and CH_4 in Electrochemical Reduction of CO_2 at Metal Electrodes in Aqueous Hydrogencarbonate Solutions. *Chem. Lett.* **1985**, *14*, 1695−1698.

(8) Yang, Y.; Ohnoutek, L.; Ajmal, S.; Zheng, X.; Feng, Y.; Li, K.; Wang, T.; Deng, Y.; Liu, Y.; Xu, D.; Valev, V. K.; Zhang, L. "Hot edges" in an Inverse Opal Structure Enable Efficient CO_2 Electrochemical Reduction and Sensitive in Situ Raman Characterization. *J. Mater. Chem. A.* **2019**, *7*, 11836−11846.

(9) Jiang, S.; Klingan, K.; Pasquini, C.; Dau, H. New Aspects of Operando Raman Spectroscopy Applied to Electrochemical CO_2 Reduction on Cu Foams. *J. Chem. Phys.* **2019**, *150*, 041718.

(10) Favaro, M.; Xiao, H.; Cheng, T.; Goddard, W. A.; Yano, J.; Crumlin, E. J. Subsurface oxide plays a critical role in CO2 activation by Cu(111) surfaces to form chemisorbed CO2, the first step in reduction of CO2. *Proc. Natl. Acad. Sci. U.S.A.* **2017**, *114*, 6706−6711.

(11) Ye, Y.; Yang, H.; Qian, J.; Su, H.; Lee, K. J.; Cheng, T.; Xiao, H.; Yano, J.; Goddard, W. A.; Crumlin, E. J. Dramatic Differences in Carbon Dioxide Adsorption and Initial Steps of Reduction between Silver and Copper. *Nat. Commun.* **2019**, *10*, 1875.

(12) Ye, Y.; Qian, J.; Yang, H.; Su, H.; Lee, K. J.; Etxebarria, A.; Cheng, T.; Xiao, H.; Yano, J.; Goddard, W. A.; Crumlin, E. J. Synergy between a Silver-Copper Surface Alloy Composition and Carbon Dioxide Adsorption and Activation. *ACS Appl. Mater. Interfaces* **2020**, *12*, 25374−25382.
(13) Todorova, T. K.; Schreiber, M. W.; Fontecave, M. Mechanistic Understanding of CO2 Reduction Reaction (CO2RR) Toward Multicarbon Products by Heterogeneous Copper-Based Catalysts. *ACS Catal.* **2020**, *10*, 1754−1768.
(14) Montoya, J. H.; Shi, C.; Chan, K.; Nørskov, J. K. Theoretical Insights into a CO Dimerization Mechanism in CO_2 Electroreduction. *J. Phys. Chem. Lett.* **2015**, *6*, 2032−2037.
(15) Nie, X.; Esopi, M. R.; Janik, M. J.; Asthagiri, A. Selectivity of CO2Reduction on Copper Electrodes: The Role of the Kinetics of Elementary Steps. *Angew. Chem., Int. Ed.* **2013**, *52*, 2459−2462.
(16) Feaster, J. T.; Shi, C.; Cave, E. R.; Hatsukade, T.; Abram, D. N.; Kuhl, K. P.; Hahn, C.; Nørskov, J. K.; Jaramillo, T. F. Understanding Selectivity for the Electrochemical Reduction of Carbon Dioxide to Formic Acid and Carbon Monoxide on Metal Electrodes. *ACS Catal.* **2017**, *7*, 4822−4827.
(17) Cheng, T.; Xiao, H.; Goddard, W. A. Reaction Mechanisms for the Electrochemical Reduction of CO2 to CO and Formate on the Cu(100) Surface at 298 K from Quantum Mechanics Free Energy Calculations with Explicit Water. *J. Am. Chem. Soc.* **2016**, *138*, 13802−13805.
(18) Xiao, H.; Cheng, T.; Goddard, W. A.; Sundararaman, R. Mechanistic Explanation of the pH Dependence and Onset Potentials for Hydrocarbon Products from Electrochemical Reduction of CO on Cu (111). *J. Am. Chem. Soc.* **2016**, *138*, 483−486.
(19) Cheng, T.; Xiao, H.; Goddard, W. A. Full Atomistic Reaction Mechanism with Kinetics for CO Reduction on Cu(100) from Ab Initio Molecular Dynamics Free-energy Calculations at 298 K. *Proc. Natl. Acad. Sci. U.S.A.* **2017**, *114*, 1795−1800.
(20) Cheng, T.; Fortunelli, A.; Goddard, W. A. Reaction Intermediates during Operando Electrocatalysis Identified from Full Solvent Quantum Mechanics Molecular Dynamics. *Proc. Natl. Acad. Sci. U.S.A.* **2019**, *116*, 7718−7722.
(21) Peterson, A. A.; Abild-Pedersen, F.; Studt, F.; Rossmeisl, J.; Nørskov, J. K. How Copper Catalyzes the Electroreduction of Carbon Dioxide into Hydrocarbon Fuels. *Energy Environ. Sci.* **2010**, *3*, 1311−1315.
(22) Calle-Vallejo, F.; Koper, M. T. M. Theoretical Considerations on the Electroreduction of CO to C2Species on Cu(100) Electrodes. *Angew. Chem., Int. Ed.* **2013**, *125*, 7423−7426.
(23) van Duin, A. C. T.; Bryantsev, V. S.; Diallo, M. S.; Goddard, W. A.; Rahaman, O.; Doren, D. J.; Raymand, D.; Hermansson, K. Development and Validation of a ReaxFF Reactive Force Field for Cu Cation/water Interactions and Copper Metal/metal Oxide/metal Hydroxide Condensed Phases. *J. Phys. Chem. A* **2010**, *114*, 9507−9514.
(24) Schouten, K. J. P.; Gallent, E. P.; Koper, M. T. M. The influence of pH on the reduction of CO and CO2 to hydrocarbons on copper electrodes. *J. Electroanal. Chem.* **2014**, *716*, 53−57.
(25) Kresse, G.; Hafner, J. Ab Initio Molecular Dynamics for Liquid Metals. *Phys. Rev. B: Condens. Matter Mater. Phys.* **1993**, *47*, 558−561.
(26) Kresse, G.; Hafner, J. Ab Initio Molecular-dynamics Simulation of the Liquid-metal-amorphous-semiconductor Transition in Germanium. *Phys. Rev. B: Condens. Matter Mater. Phys.* **1994**, *49*, 14251−14269.
(27) Kresse, G.; Furthmüller, J. Efficient Iterative Schemes for Ab Initio Total-energy Calculations Using a Plane-wave Basis Set. *Phys. Rev. B: Condens. Matter Mater. Phys.* **1996**, *54*, 11169−11186.
(28) Kresse, G.; Furthmüller, J. Efficiency of Ab-initio Total Energy Calculations for Metals and Semiconductors Using a Plane-wave Basis Set. *Comput. Mater. Sci.* **1996**, *6*, 15−50.
(29) Perdew, J. P.; Chevary, J. A.; Vosko, S. H.; Jackson, K. A.; Pederson, M. R.; Singh, D. J.; Fiolhais, C. Atoms, Molecules, Solids, and Surfaces: Applications of the Generalized Gradient Approximation for Exchange and Correlation. *Phys. Rev. B: Condens. Matter Mater. Phys.* **1992**, *46*, 6671−6687.
(30) Perdew, J. P.; Burke, K.; Ernzerhof, M. Generalized Gradient Approximation Made Simple. *Phys. Rev. Lett.* **1996**, *77*, 3865−3868.
(31) Grimme, S.; Antony, J.; Ehrlich, S.; Krieg, H. A Consistent and Accurate Ab Initio Parametrization of Density Functional Dispersion Correction (DFT-D) for the 94 Elements H-Pu. *J. Chem. Phys.* **2010**, *132*, 154104.
(32) Köhler, L.; Kresse, G. Density Functional Study of CO on Rh(111). *Phys. Rev. B: Condens. Matter Mater. Phys.* **2004**, *70*, 165405.
(33) Qian, J.; Baskin, A.; Liu, Z.; Prendergast, D.; Crumlin, E. J. Addressing the Sensitivity of Signals from Solid/liquid Ambient Pressure XPS (APXPS) Measurement. *J. Chem. Phys.* **2020**, *153*, 044709.
(34) Schouten, K. J. P.; Qin, Z.; Pérez Gallent, E.; Koper, M. T. M. Two Pathways for the Formation of Ethylene in CO Reduction on Single-crystal Copper Electrodes. *J. Am. Chem. Soc.* **2012**, *134*, 9864−9867.
(35) Becke, A. D. Density-functional thermochemistry. III. The role of exact exchange. *J. Chem. Phys.* **1993**, *98*, 5648−5652.
(36) Lee, C.; Yang, W.; Parr, R. G. Development of the Colle-Salvetti Correlation-Energy Formula into a Functional of the Electron Density. *Phys. Rev. B: Condens. Matter Mater. Phys.* **1988**, *37*, 785−789.
(37) te Velde, G.; Bickelhaupt, F. M.; Baerends, E. J.; Guerra, C. F.; van Gisbergen, S. J. A.; Snijders, J. G.; Ziegler, T. Chemistry with ADF. *J. Comput. Chem.* **2001**, *22*, 931−967.
(38) Schirmer, J.; Angonoa, G.; Svensson, S.; Nordfors, D.; Gelius, U. High-Energy Photoelectron C 1s and O 1s Shake-up Spectra of CO. *J. Phys. B: At. Mol. Phys.* **1987**, *20*, 6031−6040.
(39) Jolly, W. L.; Bomben, K. D.; Eyermann, C. J. Core-Electron Binding Energies for Gaseous Atoms and Molecules. *At. Data Nucl. Data Tables* **1984**, *31*, 433−493.

https://doi.org/10.1021/acsami.1c02909
ACS Appl. Mater. Interfaces 2021, 13, 31554−31560